De-alloying of rapidly solidified amorphous and crystalline alloys

Livio Battezzati*, Federico Scaglione

Dipartimento di Chimica IFM e Centro NIS, Università di Torino, Torino, Italy

ARTICLE INFO

ABSTRACT

De-alloying occurs when a less noble metal is selectively removed from an alloy either by chemical or electrochemical means. Under appropriate experimental conditions and for suitable alloy composition, the resulting material is constituted by crystalline ligaments rich in the noble element and pores. The literature reports a substantial amount of information on de-alloying crystalline homogeneous solid solutions, mostly based on noble metals, whereas the process has been attempted in a limited number of cases with amorphous alloys. The latter case is reviewed here and new results are given for an Au-based metallic glass evidencing the role of the critical potential and surface roughness.

It can be also of interest to remove selectively from the alloy a single phase leaving a sieve-like matrix. which might itself be porous. The size of the pores and of the remaining solid can be tailored by controlling the grain size of the phases. Examples are given for this second process and experiments are reported on successful selective etching of rapidly solidified Fe–C eutectics.

© 2011 Elsevier B.V. All rights reserved.

1. Introduction

Porous metals can be made by selective removal of a phase or an element from a bulk alloy by chemical or electrochemical means. The topic has recently gained interest for tailoring nanoporous metallic materials aiming at improved properties in various field such as catalysis, sensors, hydrogen storage, molecular sieves. The recent literature reports significant examples which can be classified according to the initial microstructure of the alloy.

De-alloying of an element from crystalline homogeneous solid solutions, mostly based on noble metals, results in the formation of a network of pores and ligaments of the remaining noble element Both experiments and models have been devised to elucidate the structure the material and the mechanism of the reactions; for a review see [1]. This process provides the finest pore size, in the nanometre range, as shown for Au–Ag [1], Au–Cu [1], Au–Sn [2], Cu–Mn [3] alloys.

Dissolution of a phase in a two phase material gives porosity of various sizes, starting typically from the micron range. Examples include Ni-base superalloys [4,5], Cu–Zr [6], Ti–Al [7]. In these, an equilibrium phase is etched away after suitable thermal or mechanical processing aimed at tailoring its size. Instead, the non-equilibrium demixing of the melt before solidification has been exploited to create phase dispersions in Cu–Co and Cu–Fe alloys [8,9] before etching. In some of these cases, the phase constitu-

tion of the material involves two solid solutions or a solution and a compound: the phase containing the less noble component is totally removed and the other phase originates a porous structure because of removal of an element as in Au–Al, made of a Au rich solid solution and an Al_2Au phase. The material has then a bimodal distribution of pore sizes [10].

De-alloying of homogeneous amorphous alloys as well as of phase separated amorphous phases, has been attempted in a number of cases with success [11–14]. Amorphous alloys contain often several components, therefore all elements but one must be removed at appropriate potential. Structural reconstruction then occurs providing a crystalline phase in all cases known to date very likely via its nucleation which can be favoured by the removal of elements which brings composition outside the glass-forming range.

The removal of a single phase from an alloy implies two steps: the design and production of a suitable microstructure and the careful use of etching methods, i.e. of Pourbaix diagrams for electrochemical techniques [1,4–9]. For obtaining porous structures by de-alloying of an element from a homogeneous solution, a substantial difference in electrochemical potential between alloy components is needed. It has then been shown that a critical potential exists for the morphology of corrosion as well as a "parting limit", i.e. a limiting content of the most noble element, usually less than that of the less noble one. Finally, the mechanisms of crystal reconstruction is based on surface and volume diffusion of the noble species or even their re-deposition from the electrolyte [5,15–18].

In this work we describe two cases falling in the above categories. The removal of a phase from a two-phase Fe–C alloy having a peculiar microstructure obtained by rapid solidification is first

* Corresponding author.
E-mail addresses: livio.battezzati@unito.it (L. Battezzati),
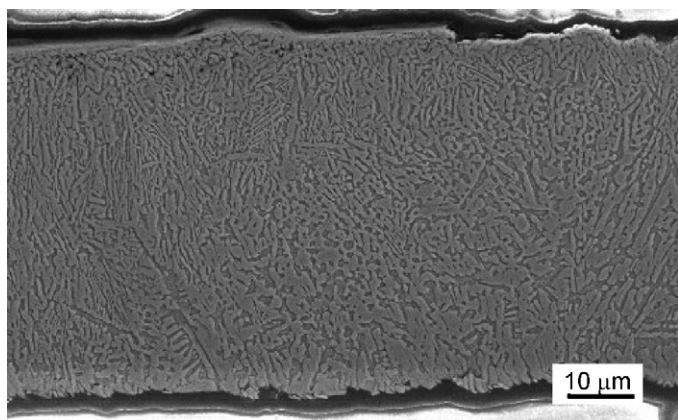federico.scaglione@unito.it (F. Scaglione).

Fig. 1. SEM image (secondary electrons) of a cross section of as-quenched 3.8 wt% C ribbon.

treated. Then, the electrochemical etching of an amorphous Au-based alloy is reported. Here, the role of the amorphous structure, of eventual embedded surface crystals, of the surface roughness must be considered in addition to the conventional electrochemical parameters [14].

2. Experimental

Fe–C ingots containing 3.8 and 4.3 wt% C and a $Au_{42}Cu_{29}Ti_8Si_{21}$ alloy were synthesized by arc melting elements of the following purity: 99.98% Fe, 99.999% C (electronic grade), 99.99% Au, 99.99% Cu, 99,9995% Si, 99.99% Ti, after evacuating and purging the furnace several times with high purity Ar and using lumps of Zr and Ti as getters. Parts of the crushed ingots were melt spun from a silica crucible onto a hardened Cu wheel under high purity Ar, obtaining ribbons 2 mm wide and 25–30 μm thick.

For electrochemical de-alloying, samples have been used as working electrode in a cell composed of a Standard Calomel reference electrode (SCE) and a Pt counter electrode in a Potentiostat/Galvanostat Model 7050, Amel Instruments.

The Fe–C alloys were etched in 14 M NaOH and 2 V, conditions suited to remove the cementite phase. The critical potential for de-alloying $Au_{42}Cu_{29}Ti_8Si_{21}$ was determined by performing anodic polarization experiments as 1.75 V. Potentiostatic and galvanostatic methods were employed with an electrolyte made of a 0.1 M HNO_3 aqueous solution; in the former, samples have been etched for 20 h at 1.80–1.90 V (versus SCE electrode), in the latter, samples have been etched at 15 mA for 6 h. During processing, the potential and current fluctuated around the average of tens of μV and units of mA, respectively.

Samples have been analysed before and after etching using X-ray diffraction (XRD) in Bragg-Brentano geometry with monochromatic Cu K alpha radiation, scanning electron microscopy (SEM), energy dispersive X-ray spectroscopy (EDS) (calibrated with a pure Co sample).

3. Results and discussion

3.1. Fe–C eutectics

Microstructural studies of binary cast irons produced with elements of high purity, have shown that the formation of the expected conventional eutectics can be kinetically suppressed by solidification at the rates achievable in the melt spinning process. A mixture of metastable cementite, slightly off-stoichiometry, and supersaturated ferrite was solidified in eutectic form from the liquid at 3.8 wt% C with the phase proportion of 61 vol% and 39 vol%, respectively [19]. Phase diagram calculation confirmed the location of the metastable eutectic. An image of a cross section of a ribbon of this alloy is reported in Fig. 1 showing the uniform eutectic microstructure. Only in thicker ribbons a transition from the microstructure of Fig. 1 to ledeburite was found.

Conditions for electrochemical etching were chosen to obtain the highest current efficiency which corresponds to oxidising the iron present in carbides to ferrate ions and carbon to carbonate ions [20]. This allows selective removal of cementite from the alloy. The
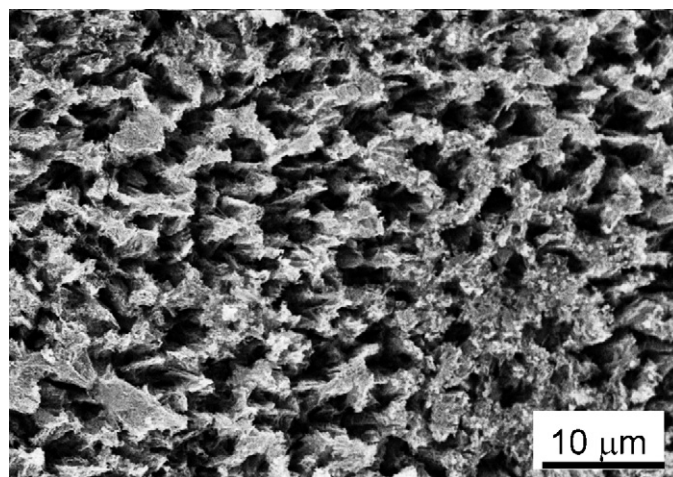

Fig. 2. SEM image (secondary electrons) of as-quenched 3.8 wt% C ribbon after electrochemical etching to remove cementite.

Fe is dissolved under the same parameter settings, although definitely more slowly, being protected to some extent by a passivating oxide film [20]. In order to remove only cementite, the etching must, therefore, be terminated at a proper stage avoiding extensive Fe corrosion. Fig. 2 shows the former air side of the ribbon which displays now widespread porosity within a Fe network. The size of the pores is on average of the order of two microns. They clearly extend into the inner part of the ribbon. Complete etching was achieved after 70 min. XRD demonstrated the material is constituted entirely by Fe.

The same electrochemical procedure was applied to slices of various thickness of an arc melted Fe–4.3% C ingot which contained fine alternate lamellae of ferrite and cementite after solidification in the proportion expected from the phase diagram. The cementite was removed and the material displayed pores one to two microns wide and of various length extending up to tens of microns (Fig. 3). The selective etching could be prolonged for various hours to obtain thick porous iron. Fig. 4 shows a view in lateral perspective of a foil, originally 80 μm thick, which appears fully etched after about 18 h at 2 V. The ferrite lamellae only remained.

It is, therefore, concluded that porous patterns of different size and shape can be obtained on account of the starting alloy microstructure.
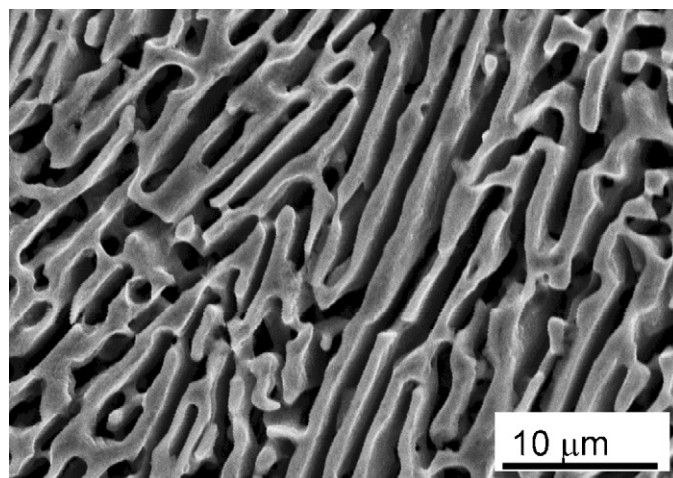

Fig. 3. SEM image (secondary electrons) of as-solidified 4.3 wt% C cast iron after electrochemical etching to remove cementite.
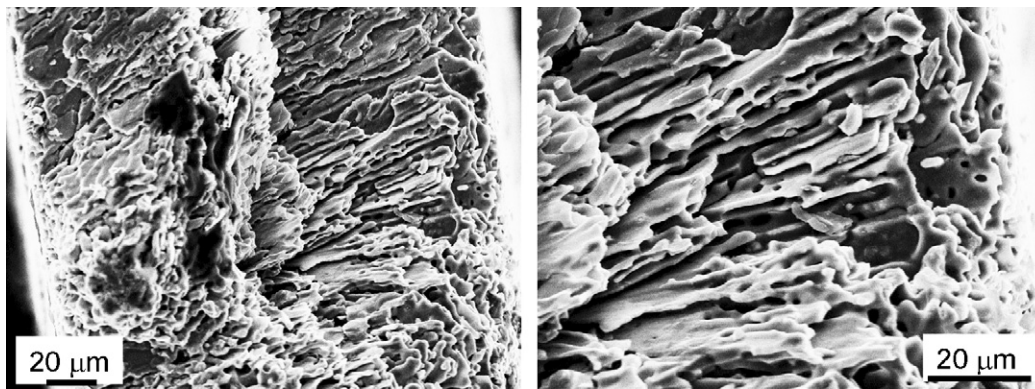
Fig. 4. SEM image (secondary electrons) of as-solidified 4.3 wt% C cast iron after prolonged electrochemical etching to remove cementite. Left: perspective view of a foil originally 80 μm thick. Right: magnification of ferrite lamellae.
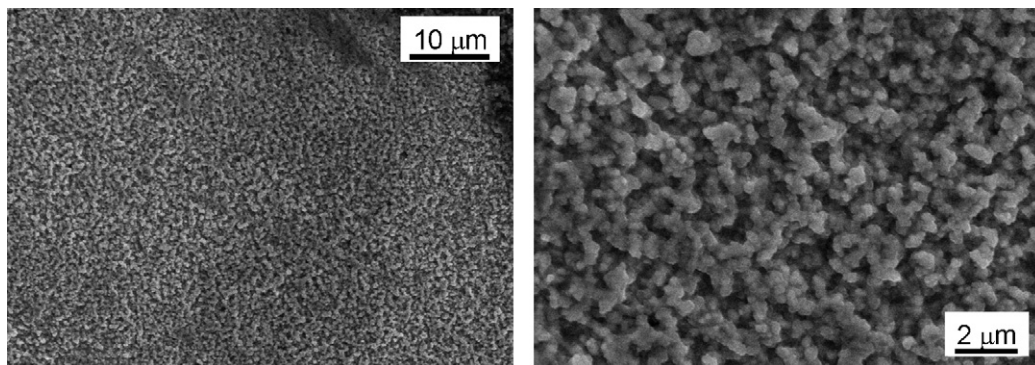

Fig. 5. SEM image of the air side of the $Au_{42}Cu_{29}Ti_8Si_{21}$ ribbon after dealloying with the potentiostatic method at 1.90 V (left). Higher magnification image on the right.

3.2. Au based amorphous alloy

The Au–Si system is the early prototype of a metallic glass-former by rapid solidification [21]. More recently, bulk metallic glasses have been obtained with atomic content $Au_{49}Ag_{5.5}Pd_{2.3}Cu_{26.9}Si_{16.3}$ [22], a composition clearly related to the Au–Cu–Si ternary eutectic. It has also been shown that the addition of Ti, having a negative heat of mixing with Au, Cu and Si, improves the glass forming ability of the ternary system, although the resulting alloy is not a bulk glass-former [23]. Among the compositions now available, $Au_{42}Cu_{29}Ti_8Si_{21}$ is below, but close to the parting limit of Au content for de-alloying. Melt spun ribbons display diverse microstructures from the amorphous wheel side to the air side where quenched-in crystals are found. These belong to a metastable cubic phase, $Cu_{15}Si_4$ type which was identified in XRD patterns by comparison with other rapidly quenched ribbons of $Au_{37.5}Cu_{37.5}Si_{25}$ composition [23,24]. These crystals are quickly removed by electrochemical etching as shown by the disappearance of their reflections from the diffraction pattern leaving an incipient porosity of micrometer size on the ribbon surface [14]. With prolonged etching at different potential above the critical one, XRD patterns show that gold rich crystals were obtained on both sides of the ribbon surfaces. Their lattice constant corresponds to that of pure gold within the data scatter [14]. SEM images of the air-side of the ribbon, show, in addition to the microporosity due to the removal of the crystalline phase, a finer porosity found in between particles of pure Au connected to each other (Fig. 5). Similar microstructure is found on the wheel-side where the general morphology of gold appears related to the pre-existing roughness of the ribbon surface with longitudinal hillocks and isolated channels (Fig. 6). The porosity extends to a layer about 5 μm thick on

both surfaces. Galvanostatic experiments provided similar morphology of gold [14].

Crystals and porosity displayed different morphology as a function of applied potential. With potential just above the critical value (e.g. 1.80 V), the appearance of the surfaces is more patchy. Some areas are close in morphology to those just described, whereas others contain gold of different shapes. This is more evident on the wheel side as shown in Figs. 7–9. The surface displays corrosion cracks and island of Au (Fig. 7). These are more clearly seen in the magnified image of Fig. 8. Cracks can be associ-
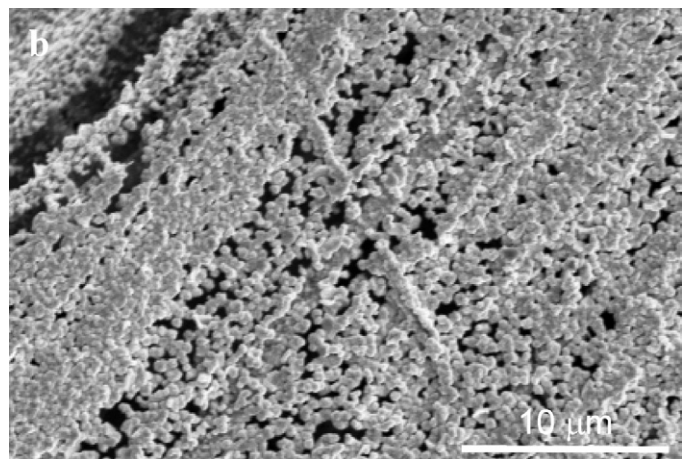

Fig. 6. SEM image of the on the wheel-side of the $Au_{42}Cu_{29}Ti_8Si_{21}$ ribbon after dealloying with the potentiostatic method at 1.90 V. Porous gold with longitudinal hillocks and isolated channels.
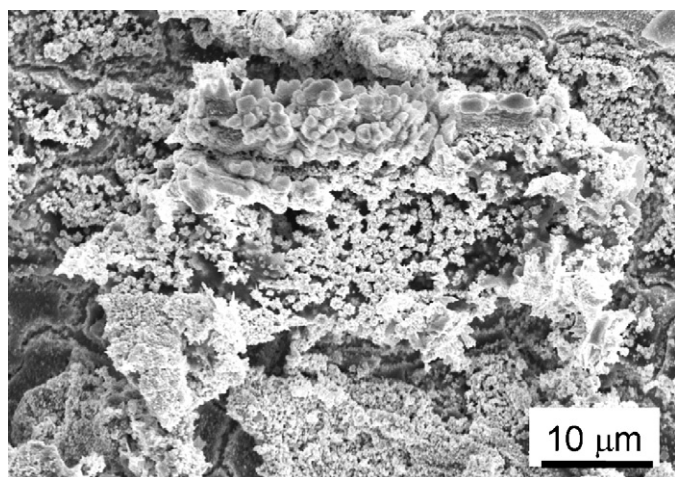
Fig. 7. SEM image of the on the wheel-side of the $Au_{42}Cu_{29}Ti_8Si_{21}$ ribbon after dealloying with the potentiostatic method at 1.80 V. Corrosion cracks and Au islands.
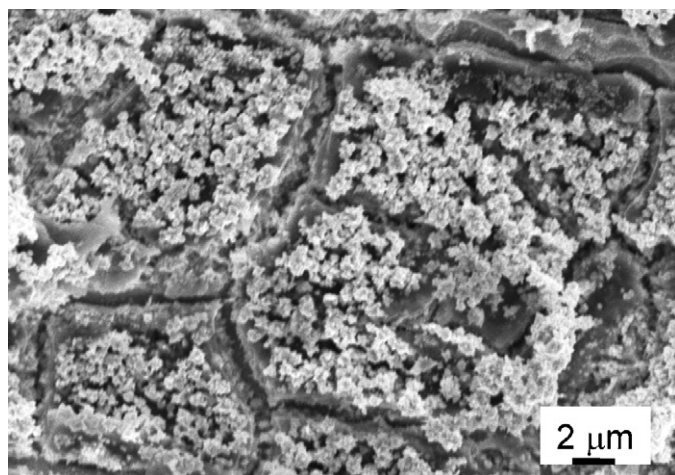

Fig. 8. Magnification of part of Fig. 7 showing corrosion cracks and locally re-deposited Au.

ated to stress corrosion and to the misfit and volume reduction between the de-alloyed layers and the underlying alloy. Au particles appear deposited on top of the islands. A closer inspection of some of them reveals that they are layered instead of porous
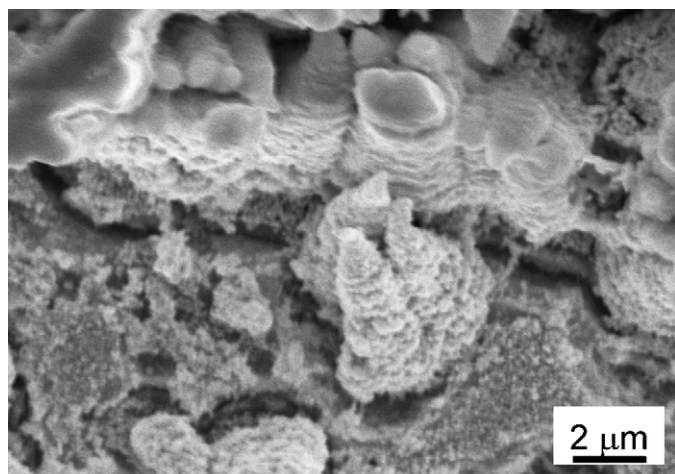

Fig. 9. Magnification of part of Fig. 7 showing re-deposited Au in layer form.

(Fig. 9). This is clearly indicative of a different growth mechanism with respect to the previous ones (Figs. 5 and 6). The mechanism of formation of Au crystals must involve a first stage, common to all cases shown here, in which nucleation of crystals occurs very likely heterogeneously on emerging asperities, contrary to de-alloying of crystalline alloys which are composed already of a single face-centered cubic phase. Then, the microstructure of Figs. 5 and 6 made of three dimensional aggregates of gold particles implies surface diffusion of gold when the less noble elements are dissolved. Volume diffusion of Au to the surface could also be invoked, but it is less likely to be effective: in fact, it should cause the formation of crystallization products of the alloy of which no evidence was ever encountered. Instead, the morphology of Figs. 7–9 is compatible with local passivation due to noble element layers and elemental re-deposition from the electrolyte possibly because of fluctuations of the potential around the critical value [25].

Microanalysis has been performed on both sides of uniform areas of the de-alloyed ribbons showing surface enrichment in gold and depletion in copper while the titanium and silicon percentage was on average decreased less. This results are not in contradiction with the XRD results that shows reflections of pure gold after de-alloying: microanalysis data give an average composition between the de-alloyed layer, made of pure gold, and the layers below that have not been etched yet. Elemental maps and fine spot EDS analyses showed enrichment of Si and Ti in the pores accompanied by higher Oxygen signal. A current density of the order of tens of mA/cm^2 was recorded in different experiments. It then decreased progressively at all potentials as a function of time becoming almost halved after about 50 min remaining then substantially constant during the etching time (20 h). This passivating effect is likely due to both surface gold enrichment and progressive coverage and to enrichment in Si and Ti possibly as oxides in the pores. As expected from the respective Pourbaix diagrams, Si and Ti de-alloy first, however, after pores formation their removal is less effective due to a passivation effect. The de-alloyed thickness is, nevertheless, substantial and the remaining ribbon help in further manipulation of the material.

Having verified the feasibility of de-alloying of amorphous metallic phases, the mechanism at atomic level is not disclosed, however, and would need detailed examination of the early stages of the process.

4. Conclusions

The present work shows that porous patterns of different size and shape can be obtained on account of the starting alloy microstructure in Fe–C eutectics providing a cheap mean to obtain materials for catalysis and sieving.

De-alloying of a partially crystalline/amorphous alloy has been performed obtaining porosity of different size. Porous gold networks have been obtained from crystalline alloys in many instances [1–3] containing often finer pores, i.e. in the tens of nanometre range, than those shown in Figs. 5–9. The larger Au crystals obtained here can be related to the alloy composition close to the parting limit for de-alloying although necessary for glass formation. The role of the initial amorphous structure does not appear decisive. On removing the less noble components, nucleation of gold crystals must be very quick, being facilitated by local heterogeneity and the apparent fast surface diffusion. Using glassy alloys, de-alloying could, however, be interesting to obtain a starting single phase in cases when no crystalline homogeneous phase can be obtained and to promote patterns by controlled crystallisation.

Acknowledgements

References

[1] J. Erlebacher, R. Seshadri (Eds.), MRS Bull. 34 (8) (2009) 561–566.

[2] S. Hu, W. Huang, Z. Li, Mater. Lett. 64 (2010) 1257–1260.

[3] J.R. Hayes, A.M. Hodge, J. Biener, A.V. Hamza, K. Sieradzi, J. Mater. Res. 21 (2006) 2611–2616.

[4] J. Rösler, D. Mukherji, Adv. Eng. Mater. 5 (12) (2003) 916–918.

[5] Y.N. Li, Z.P. Xi, X.T. Kang, H.P. Tang, W.Y. Zhang, J. Zhang, G.Z. Li, Intermetallics 17 (2009) 1065–1069.

[6] H.-B. Lu, Y. Li, F.-H. Wang, Scripta Mater. 56 (2007) 165–168.

[7] Y. Koizumi, A. Sugihare, H. Tsuchiya, Y. Minamino, S. Fujimoto, H. Yasuda, M. Yoshiya, Acta Mater. 58 (2010) 2876–2886.

[8] L. Battezzati, S. Curiotto, E. Johnson, N.H. Pryds, Mater. Sci. Eng. A 449–451 (2007) 7–11.

[9] B.J. Park, Y.M. Chen, T. Ohkubo, Intermetallics 17 (2009) 958–961.

[10] Z.-H. Zhang, Y. Wang, Z. Qi, C. Somsen, X.-G. Wang, C.-C. Zhao, J. Mater. Chem. 19 (2009) 6042–6050.

[11] J. Yu, Y. Ding, C. Xu, A. Inoue, T. Sakurai, M. Chen, Chem. Mater. 20 (2008) 4548–4550.

[12] H. Abe, K. Sato, H. Nishikawa, T. Takemoto, M. Fukuhara, A. Inoue, Mater. Trans. 50 (2009) 1255–1258.

[13] J. Jayarai, J.M. Park, P.F. Gostin, E. Fleury, A. Gebert, L. Schultz, Intermetallics 17 (2009) 1120–1123.

[14] F. Scaglione, A. Gebert, L. Battezzati, Intermetallics 18 (2010) 2338–2342.

[15] J. Erlebacher, M.J. Aziz, A. Karma, N. Dimitov, K. Sieradzki, Nature 410 (2001) 450–453.

[16] M. Stratmann, M. Rohwerder, Nature 410 (2001) 420–423.

[17] K. Sieradzki, N. Dimitov, D. Movrin, C. McCall, N. Vasiljievic, J. Erlebacher, J. Electrochem. Soc. 149 (2002) B370–B377.

[18] J. Erlebacher, J. Electrochem. Soc. 151 (2004) C614–C626.

[19] L. Battezzati, M. Baricco, S. Curiotto, Acta Mater. 53 (2005) 1849–1856.

[20] K. Bouzek, H. Bergmann, Corros. Sci. 41 (1999) 2113–2128.

[21] W. Klement Jr., R.H. Willens, P. Duwez, Nature 187 (1960) 869.

[22] J. Schoers, B. Lohwongwatana, W.L. Johnson, A. Peker, Appl. Phys. Lett. 87 (2005) 061912.

[23] G. Fiore, L. Battezzati, Rev. Adv. Mater. Sci. 18 (2008) 190–192.

[24] G. Fiore, I. Ichim, L. Battezzati, J. Phys.: Conf. Ser. 144 (2009) 012039.

[25] K. Wagner, S.R. Brancovic, N. Dimitrov, K. Sieradzki, Electrochem. J. Soc. 144 (1997) 3545–3555.